DEUTSCHES ELEKTRONEN-SYNCHROTRON DESY

DESY SR-81/15
December 1981

MILLI-EV ENERGY RESOLUTION IN BRAGG BACKSCATTERING

by

W. Graeff and G. Materlik
Hamburger Synchrotronstrahlungslabor HASYLAB
at
Deutsches Elektronen-Synchrotron DESY, Hamburg

NOTKESTRASSE 85 · 2 HAMBURG 52

To be sure that your preprints are promptly included in the
HIGH ENERGY PHYSICS INDEX ,
send them to the following address (if possible by air mail) :

DESY
Bibliothek
Notkestrasse 85
2 Hamburg 52
Germany

DESY SR-81/15
December 1981

MILLI-EV ENERGY RESOLUTION IN BRAGG BACKSCATTERING

W. Graeff
G. Materlik

Hamburger Synchrotronstrahlungslabor HASYLAB
at
Deutsches Elektronensynchrotron DESY
2000 Hamburg 52, Germany.

to be published in
Proceedings of the National Conference on Synchrotron Radiation
Instrumentation, Ithaca, New York, July 1981

ABSTRACT

We have measured the width of single crystal reflection curves and the corresponding energy resolution at an extreme back reflection angle $\Theta_B = \pi/2 - 2.86$ mrad by using a double crystal spectrometer with two separate (111) silicon crystals. The energy of the fundamental is $E_{111} = 1.98$ keV. Higher orders up to $E_{12\ 12\ 12} = 23.76$ keV were registered with an intrinsic Ge solid state detector. The results have been compared with theoretical calculations using a reformulated dynamical theory and including the source parameters of DORIS. The overall agreement is very good.

1.0 INTRODUCTION

High photon fluxes which are available from storage rings have recently stimulated discussions about the feasibility to carry out inelastic X-ray scattering experiments with an energy resolution in the range of 1 -100 meV. In comparison to neutrons X-rays have a larger cross section. This can in turn allow studies of smaller samples or even of surfaces [1]. Also, the range of energies above 100 meV is not easily accessible for neutrons so that studies of phonon modes in this energy range become possible with X-rays [2].

In order to decide whether this kind of experiments can be performed at existing or planned dedicated synchrotron radiation sources a number of questions have to be answered beforehand.

- Does the Dynamical Theory of X-ray diffraction still hold at Bragg angles close to 90°?
- Are crystals available which are good enough for monochromators?
- Which geometric factors of the source can critically limit the realizable photon flux on the sample and the corresponding energy resolution?

Following these important points a reformulation of von Laue's Dynamical Theory is presented in chapter 2. Special attention is paid to the case of $\Theta_B \sim 90°$. To compare these results with reality a double crystal spectrometer was used in back reflection geometry. Details of the experiment are described in chapter 3 and are compared with the theory in chapter 4.

2.0 DYNAMICAL THEORY OF BRAGG BACKSCATTERING

The Dynamical Theory of X-Ray scattering as developed by von Laue [3] leads to a system of linear equations for the amplitudes of the Bloch waves representing the photon inside the crystal. In principle an infinite number of Bloch waves can contribute to the solution. The first step to solve these equations is to find the shape of the dispersion surface from the secular determinant of the system. The dispersion surface is formed by all those wave vectors $\boldsymbol{K}$ which are allowed inside the crystal for a given energy E (or vacuum wave number k). Far away from any Bragg reflection the dispersion surface is simply a sphere around the reciprocal lattice point under consideration. In the two beam case where two Bloch waves dominate two such spheres penetrate each other which leads to a splitting of the dispersion surface along the intersection line.

In the conventional theory this case is approximated by neglecting the curvature of the spheres i.e. taking the tangents instead which leads to sufficiently accurate results as long as the scattering angle is far enough away from 0° and 90°. The dispersion surface, now a simple hyperbola, considerably deviates from the asymptotes in a region of the order of $k|\chi_h|$ around the intersection line. χ_h is the Fourier coefficient of the dielectric susceptibility and typically of the order of 10^{-5} to 10^{-7}.

Approaching a scattering angle of 90° the apices of the two spheres come closer to this critical distance $k|\chi_h|$ leading to a deformation of the hyperbolic shape of the dispersion surface. The concept of replacing the spheres by their tangents is obviously no longer meaningful.

To treat the backscattering case properly one has to start from the secular equation

$$(1) \qquad \begin{vmatrix} \dfrac{K_0^2 - k^2}{K_0^2} - \chi_0 & -\chi_{\bar{h}} \\ -\chi_h & \dfrac{K_h^2 - k^2}{K_h^2} - \chi_0 \end{vmatrix} = 0$$

without neglecting quadratic terms. This leads to a fourth order equation for the dispersion surface as already demonstrated by Brümmer et al. [4].

*** Figure 1 here ***

Figure 1. : Definition of the (u,v) coordinate system and illustration of ψ-scan and E-scan in k-space.

Figure 1 defines the coordinate system (u,v) which is centered between the reciprocal lattice points 0 and H which represent the scattering vector g_h with modulus $g = |g_h|$. The wave vectors K_0 and K_h inside the crystal are expressed in the new coordinates

$$(2) \qquad K_0^2 = u^2 + (v - g/2)^2$$

$$(3) \qquad K_h^2 = u^2 + (v + g/2)^2$$

With the abbreviations

(4) $\alpha = \chi_h\chi_{\bar{h}}/(1 - \chi_0)^2$

(5) $g^2/4 + \Delta = k^2/(1 - \chi_0)(1 - \alpha)$

we define a parameter of incidence y which will replace the conventional parameter used in Zachariasen's notation [5] as will be seen later on.

(6) $y = 4\,(u^2 - \Delta)/g^2\sqrt{|\alpha|}$

Using (2) - (6) equation (1) yields

(7) $(v^2 + {}^1/_4\, g^2\sqrt{|\alpha|}\, y)^2 - v^2g^2 = \alpha(g^2/4 + \Delta)^2.$

The exact solution of (7) is

(8) $v^2 = {}^1/_2\, g^2 \left[1 - {}^1/_2\sqrt{|\alpha|}\, y - \sqrt{1 - \sqrt{|\alpha|}\, y + \alpha\,({}^1/_2 + 2\Delta/g^2)^2}\right]$

(the solution with the positive sign of the root has been ruled out for physical reasons.) For $\sqrt{|\alpha|}\, y \sim |\chi_h|\, y << 1$, $\Delta << g^2$ we find the approximation

(9) $v^2 \sim {}^1/_{16}\, g^2\, |\alpha|\, (y^2 - \alpha/|\alpha|)$

With $\nu^2 = \alpha/|\alpha|$ we finally have

(10) $v_{1,2} \sim \pm {}^1/_4\, g\, \sqrt{|\alpha|}\, \sqrt{y^2 - \nu^2}$

Including absorption by complex values of χ_0 and χ_h, y and $v_{1,2}$ are also complex quantities. For constant k the imaginary part of y is constant. The real part is proportional to the square of the angular deviation ψ from normal incidence and to first order depends linearly on the deviation δk of k from $k_0 = g/2$, the wave number for normal incidence.

The amplitude ratio $\xi = D_h/D_0$ can now be calculated from the fundamental equations. To a good approximation we find

$$(11)\quad \xi_{1,2} = \frac{1 - \chi_0}{|1 - \chi_0|}\,\frac{\sqrt{|\chi_h\chi_{\bar{h}}|}}{\chi_{\bar{h}}}\,(y \pm \sqrt{y^2 - \nu^2})$$

which is essentially the same formula known from the conventional theory. But there y depends linearly on the angular deviation.

In order to calculate the transmitted and reflected intensities from a plane parallel crystal plate of thickness t one has to fulfill the boundary conditions. It turns out that with the redefined y we get the same arithmetic expressions for the continuity of wave vector components as already known from the conventional theory. Hence we can directly take the final results for the amplitude ratios of incoming and outgoing waves from [6]:

(12) transmission

$$D_0^s/D_0^i = \langle 0|1,2|0\rangle_B = \exp(ia_0t + iAy)[C + iyS]^{-1}$$

(13) reflection

$$D_h^s/D_0^i = \langle 0|1,2|h\rangle_B = i\,\chi_h/\sqrt{\chi_h\chi_{\bar{h}}}\cdot\exp(i(a_{rh}-a_{r0})z_f - 2\pi i z_f y_r/\Delta_e)\cdot S\,[C + iyS]^{-1}$$

with

(14) $S = \sin(A\sqrt{y^2 - \nu^2})/\sqrt{y^2 - \nu^2}$

(15) $C = \cos(A\sqrt{y^2 - \nu^2})$

(16) $A = \pi t/\Delta_e$

where $\Delta_e = 2/g\sqrt{|\alpha|}$ is the extinction length for the backscattering case and

(17) $a_0 = -a_h = \pi\chi_0(g/2 + 2\Delta_e/g).$

z_f is the distance of the origin of real space to the entrance surface of the crystal which is assumed to be parallel to the u-axis. Eq.(12) and (13) reveal the wellknown Pendellösung oscillations for thin crystals.

*** Figure 2 here ***

Figure 2. : Dispersion surface for the real part of the wave vectors inside the crystal and single reflection curves R (ψ-scans and E-scans) for different energies. Note that the v-scale is enlarged by a factor of 500 with respect to the u-scale. For the example at the bottom the geometrical construction of the ψ-scan from the E-scan is indicated by dashed lines. $\delta k = k - g/2$. (The discussion is given in the text.)

We shall give now a simple interpretation of the behaviour of single reflection curves near 90° as they have first been calculated in [4] but without pendellösung effects. Figure 1 shows the region in k-space around the origin of the (u,v) system and illustrates the two different ways of scanning through k-space, namely the angular scan (ψ-scan) and the energy scan (E-scan). Figure 2 shows a few examples. The E-scan is almost independent of ψ and as y varies linearly with E it has always the same shape. On the contrary the ψ-scan strongly depends on E. Figure 2 also demonstrates how one can easily find the complex shape of the ψ-scan from the shape of the E-scan by simple geometrical transformation without knowing the shape of the dispersion surface. It is easy to show that all lines with constant v of the incoming wave vector have a constant y. As the reflected intensity only depends on y we can immediately tell that all incoming waves with k vectors ending on a parallel to the u-axis have the same reflectivity. For some applications it might be interesting that for energies where the asymptotes no longer intersect only wavefields with y>0 can exist which undergo the anomalously low absorption.

With $\psi \sim u/k_0$ and neglecting higher order terms we find from eqs.(4)-(6)

(18) $$y \sim (\psi^2 - 2\delta k/k_0 - \chi_0)/|\chi_h|$$

For a fixed ψ the shift $\delta k = k - k_0$ at the center of the total reflection range ($y_r = 0$) is found to be

(19) $$\delta k = {}^1/_2\, k_0(\psi^2 - \chi_0)$$

As in the conventional theory total reflection occurs in the range $|y| \leq 1$ which corresponds to a spread

(20) $$\Delta k = k_0|\chi_h|$$

in wave number. This spread which is directly related to the energy resolution via $\Delta k/k_0 = \Delta E/E$ is to first order independent of the incident angle. But this is only true for plane waves close to normal incidence. In reality with a given solid angle the energy is smeared out when going away from normal incidence. The choice of the shape of the solid angle is very essential in experiments aiming at high energy resolution. At $\psi \neq 0$ obviously a ring aperture centered about the normal of the reflecting planes would be ideal for maximum intensity at maximum energy resolution because ψ does not change with the azimuth angle. Let ψ^+ and ψ^- be the upper and lower boundaries of such an aperture so we can define the width by $\Delta\psi = \psi^+ - \psi^-$and the center $\langle\psi\rangle = (\psi^+ + \psi^-)/2$. The best choice for $\Delta\psi$ at a given wave number k is the angular width of the total reflection which is

(21) $$\Delta\psi = |\chi_h|/\langle\psi\rangle$$

It is interesting to note that one can keep the energy resolution and the intensity constant when increasing $\langle\psi\rangle$ and decreasing $\Delta\psi$ in such a way that the total cross section of the aperture which is proportional to $\Delta\psi\langle\psi\rangle$ is kept constant.

As the ring aperture requires either a ring shaped sample or detector it might be more convenient to use a rectangular aperture. From the above considerations one can immediately tell the appropriate orientation and height to width ratio of such an aperture. A rectangular slit of width $\Delta\psi_w$ should cut out of the ring aperture as much as possible leading to an optimum height $\Delta\psi_h$ of

(22) $$\Delta\psi_h = 2\sqrt{2\langle\psi\rangle\,\Delta\psi_w - (\Delta\psi_w)^2} = 2\sqrt{2\,|\chi_h| - |\chi_h|^2/\langle\psi\rangle^2}$$

For Si 888 with $|\chi_h| = 2.6\cdot10^{-7}$ we find for $\langle\psi\rangle = 2.6$ mrad a slit width of $\Delta\psi_w = 0.1$ mrad and a slit height $\Delta\psi_h = 1.4$ mrad.

The total number of photons reflected into a solid angle $\Delta\Omega$ is regardless of its shape

(23) $$N = I\, R_i^E\, \Delta\Omega$$

where I is the number of photons per unit energy per unit solid angle and $R_i^E = \int R(E)\, dE$ is the integrated reflectivity for constant ψ. R_i^E is a constant for each reflection which can be calculated from the conventional theory

(24) $$R_i^E = {}^1/_2\, |\chi_h|\, E\, R_i^y = {}^1/_2\, \Delta E\, R_i^y$$

where R_i^y is the parameterized integral reflectivity in the Bragg case. R_i^y ranges in the case of silicon from 2.0 to 2.3 and we have approximately $R_i^E \sim \Delta E$.

*** Figure 3 here ***

Figure 3. : Compilation of several combinations R_i^E versus E which are possible with silicon reflections. As $R_i^E \sim \Delta E$ it shows that the energy resolution increases with the magnitude of the scattering vector.

*** Figure 4 here ***

Figure 4. : Photon fluxes available from DORIS for the reflections shown in Figure 3. No corrections are made for absorption in windows and for finite source size.

Figure 3 is a plot of most combinations R_i^E versus E which are possible with Si reflections. With Ge each combination would have a slightly lower energy and a nearly three times larger R_i^E. Figure 4 shows for these combinations the corresponding photon fluxes calculated for DORIS running at 3.5 GeV.

It is important to note that 111 and 220-reflections are the only pure two beam cases at $\Theta_B = 90°$. In general complex many beam cases occur which are restricted to an angular range of several times the corresponding Fourier coefficients. Compared to the large angular width of the back reflection their effect may be neglected in most practical cases.

3.0 EXPERIMENTAL METHOD.

A double crystal diffractometer was installed in back reflection geometry with $\Theta_B = 90° - 2.86$ mrad in the EMBL laboratory at the storage ring DORIS.

*** Figure 5 here ***

Figure 5. : Scheme of the experimental setup at DORIS. Beam path is projected into the horizontal plane (see text).

The arrangement is sketched in Figure 5. The first crystal was placed 36 m away from the tangent point of the orbiting positrons. Two successive perfect dislocation-free silicon crystals with (111) reflections were arranged in a geometry which is conventionally called a dispersive (+,+) diffractometer setting. However, for geometrical reasons the first crystal was reflecting downwards and the second upwards. Their reflection planes enclosed an angle of about 60°. We describe this setup by the abbreviation (+,+,60°). The same crystal material was tested before by producing X-ray interferometers. In that application it proved to have a variation in lattice spacing $\Delta d/d < 5 \cdot 10^{-8}$.

The crystals were placed 7 m apart from each other in order to achieve a sufficient distance between second crystal and primary beam. The direct synchrotron radiation beam was collimated by a pinhole of 0.2 mm diameter which was centered approximately in the maximum of the vertical distribution of synchrotron X-rays.

The first crystal was aligned perpendicular to the incident beam by taking successive Laue patterns in back reflection geometry. Their asymmetry revealed the misalignment. By using this simple procedure we neither needed to operate a detector at the place of the second crystal nor did we have to perform time consuming two-dimensional angular scans to find the reflection. The fine tuning of the once reflected beam onto the second crystal was finished with successive photographs taken at the place of the second crystal.

The twice reflected beam was recorded and analyzed by an intrinsic germanium solid state detector (SSD) connected to a multichannel analyzer. A large diameter (25 cm) evacuated beam tube filled the gap between the crystals to reduce air absorption.

*** Figure 6 here ***

Figure 6. : Typical spectrum of the double reflected beam at the center of the rocking curve taken with a solid state detector.

Figure 6 shows a typical spectrum which was detected at the maximum of the rocking curve. Even the 12th harmonic of the 111-reflection is clearly visible at 23.4 keV. The lower energy lines are missing because of rest absorption in air and in beam pipe windows. In conjunction with the spectral distribution of DORIS (which was running at 4.38 GeV) and with the efficiency of the SSD this absorption leads to the dominance of the 888-reflection in this spectrum.

For a fixed angle of the first crystal we performed an angular scan by rotating the second crystal and translating the detector to record a rocking curve. The energy bandwidth of the highly monochromatic radiation was measured by changing the lattice constant d via temperature T of the second crystal. A change ΔT was induced by heat irradiated from a light bulb and measured by a Fe-Constantan thermocouple. The reflected intensity was registered as a function of temperature on an x-y recorder. The energy bandwidth ΔE^d was determined by using the relation

$$\Delta E^d/E = \Delta d/d = \alpha_{Si}\,\Delta T$$

with $\alpha_{Si} = 3 \cdot 10^{-6}\ grd^{-1}$.

4.0 EXPERIMENTAL RESULTS

4.1 ROCKING CURVES

Figure 7 shows rocking curves of four different harmonics which have been measured in the way described above. This angular scan reflects the ψ-scan in Figure 2 for a constant energy $E_0 \pm \Delta E/2$. Two such single crystal reflection curves, however, are convoluted with each other in the experiment. Furthermore, that product is convoluted with the source emittance which in turn is determined by the natural width $\sigma_{z,nat}'$ of the synchrotron radiation cone and by the width $\sigma_{z,e}'$ of the vertical momentum distribution of the orbiting positrons. Also, even at $\Theta_B \sim 89.84°$, the horizontal and vertical source size (σ_x, σ_z) still contribute to the width of the rocking curves because they are registered in a dispersive spectrometer mode.

reflection	width (FWHM)	
	theory	experiment
777	46"	45.4"
888	40"	41.8"
999	30"	34.6"

Table 1 Comparison of rocking curve widths for three different harmonics. Following parameters were used for the calculation: geometry (+,+,90°), $2.35 \cdot \sigma_{z,nat}' = 0.16$ mrad, $2.35 \cdot \sigma_{z,e}' = 0.4$ mrad, $2.35 \cdot \sigma_x = 3$ mm, $2.35 \cdot \sigma_z = 2.5$ mm, $\psi = 2.86$ mrad, $\Delta\psi_w = \Delta\psi_h = 8$ μrad.

Table 1 demonstrates the very good agreement between the calculated and measured rocking curve widths. The intensity profile of the synchrotron radiation cone was explicitly included from Schwinger's formula. $\sigma_{z,e}'$ was estimated from beam optic parameters. σ_x and σ_z could be measured directly in the geometry shown in Figure 5. The small entrance slit serves nicely for a pinhole camera if a film replaces the SSD. These beam parameters characterize Gaussian profiles which have been used for the calculation.

*** Figure 7 here ***

Figure 7. : Rocking curves of four different harmonics of the 111-reflections measured by rotating the second crystal. The inset shows "E-scans" performed by changing the temperature of the second crystal to determine the energy bandwidth.

4.2 ENERGY BANDWIDTH

The inset of Figure 7 displays the intensity change of the 888-reflection when the temperature of the second crystal is altered by about 0.3° C. The measured full width at half maximum (FWHM) is $\Delta E^d_{888} = 8.3$ meV or $(\Delta E^d/E)_{888} = 5.3 \cdot 10^{-7}$.

geometry	ΔE^d_{888} [meV]		I_{888} [phot/sec]	
	theory	exp.	theory	exp.
(+,-)	6.0		16000	
(+,+,90)	8.5		11000	
(+,+,180)	10.0		8400	
(+,+,60)		8.3		8200

Table 2 Comparison of calculated and measured energy bandwidth ΔE^d measured by T variation and of intensity I for the 888-reflection and different geometries. Parameters are the same as for Table 1. Intensity normalized to 4.38 GeV and 10 mA.

The compilation in Table 2 indicates the variation of ΔE^d for different geometric configurations. The agreement between the calculated value (+,+,90°) and the measured one at (+,+,60°) is good within the experimental errors indicated in Figure 7. The table also demonstrates the range of resolution in a double crystal spectrometer which can simply be covered by altering the geometry from (+,-) to (+,+,180°). The lowest limit which can in principle be achieved behind one crystal with this reflection is set by the intrinsic width at 15.82 keV which is 4.1 meV or $\Delta E/E = 2.59 \cdot 10^{-7}$.

4.3 INTENSITIES

The maximum intensities of the rocking curves in Figure 7 were corrected for absorption in air and beam tube windows. A normalization to 10 mA current and a rectangular slit of 8 μrad horizontal and 8 μrad vertical width allowed a direct comparison of the calculated and measured values as compiled in Table 2. If we compare the values for (+,+,90°) and (+,+,60°) the close agreement is again obvious. Here is $I_{Theory}/I_{Exp.} = 1.3$. If we take the error bar for $\sigma_{I,i}$ into account no better agreement can be expected.

5.0 CONCLUSIONS

It was experimentally demonstrated that an extended Dynamical Theory is adequate to describe Bragg backscattering with respect to width of rocking curves, transmitted energy bandwidth and reflectivity. However, the dependance on source characteristics like divergence and shape has to be treated in a proper way. Easily accessible are energy resolutions in the meV range by choosing the appropriate reflection and crystal material. Care has to be taken in estimating the photon flux which is available from a specific storage ring. In our case, taking the number from Table 2 and choosing optimum conditions a flux of about 10^8 phot./sec can illuminate a 1 mm^2 large sample in a bandwidth of several meV. This assumes that DORIS runs with a current of about 100 mA. Such a primary monochromator can be coupled very advantageously into the structure of the storage ring. The first crystal has to be placed very close to the ring to reflect the light by 180° back through the same tangent point where it was generated into a beampipe leading to an experimental station. If the storage ring runs in a dedicated mode with one kind of particles only, this line would be free of background radiation.

We like to conclude this paper by pointing out that with existing storage rings one to two orders of magnitude higher fluxes can be reached by focusing optics or by use of wigglers. A dedicated ring like the ESRF for example [7] can produce an increase in intensity by another factor of 10 on the same 1 mm^2 sample because of its smaller source size and higher current.

6.0 REFERENCES.

[1] D.E. Moncton, J.B. Hastings, private communication, 1980.

[2] B. Dorner, private communication, 1981.

[3] M. von Laue, "Röntgenstrahlinterferenzen," Akademische Verlagsgesellschaft, Frankfurt a.M. 1960.

[4] O. Brümmer, H. R. Höche, J. Nieber, phys. stat. sol. (a) 53, 565-570 (1979).

[5] W.H. Zachariasen, "Theory of X-Ray Diffraction in Crystals," Dover Publications,New York,1967.

[6] U. Bonse, W. Graeff in "X-Ray Optics," ed. H. J. Queisser, Topics in Appl. Phys. vol. 22, pp 93-143, Springer Verlag Berlin 1977.

[7] B. Buras, G.V. Marr, eds. of "European Synchrotron Radiation Facility" a design study, Suppl. III, European Science Foundation, Strasbourg, 1979.

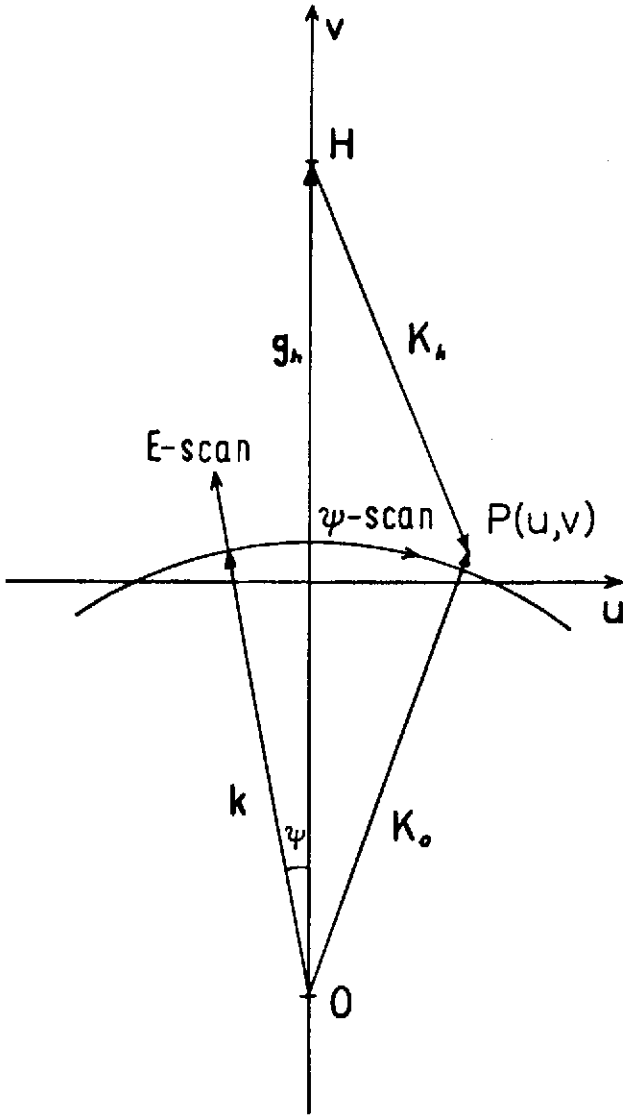
v
H
g_h
K_h
E-scan
ψ-scan
P(u,v)
u
k
ψ
K_o
O

Fig. 1

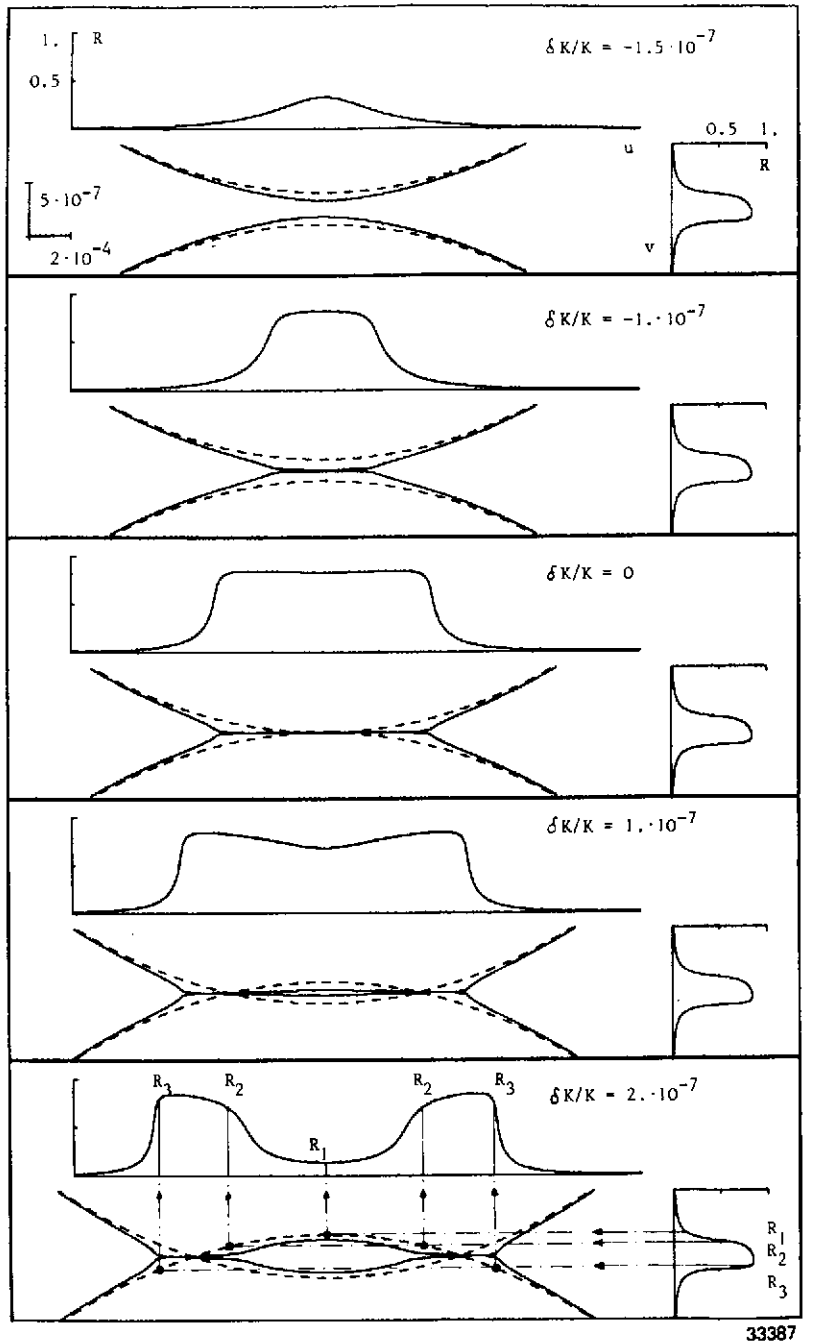
1.
R
0.5
δK/K = -1.5·10⁻⁷
0.5 1.
R
u
5·10⁻⁷
2·10⁻⁴
v
δK/K = -1.·10⁻⁷
δK/K = 0
δK/K = 1.·10⁻⁷
R3 R2 R2 R3
R1
δK/K = 2.·10⁻⁷
R1
R2
R3
33387

Fig. 2

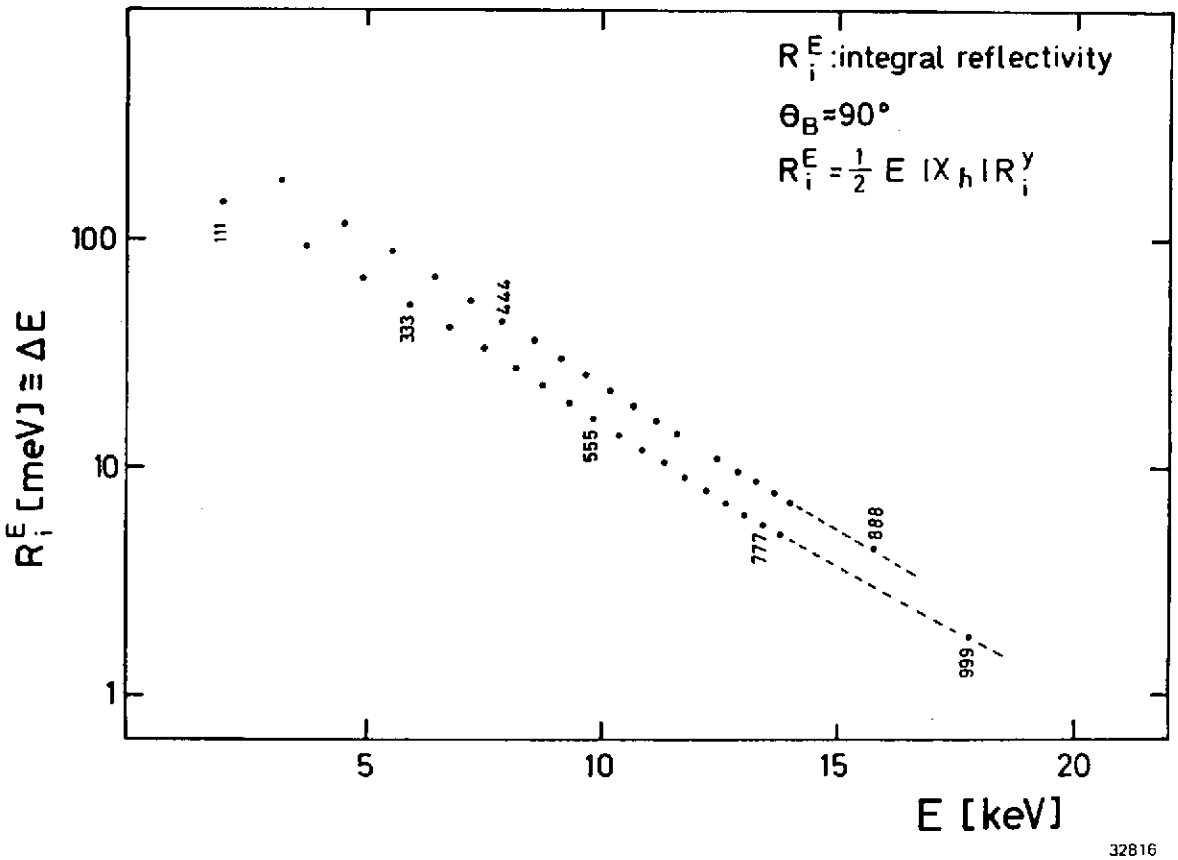
R_i^E :integral reflectivity
Θ_B=90°
$R_i^E = \frac{1}{2} E\ |X_h|\ R_i^y$
R_i^E [meV] ≡ ΔE
100
10
1
111
333
444
555
777
888
999
5
10
15
20
E [keV]
32816

Fig. 3

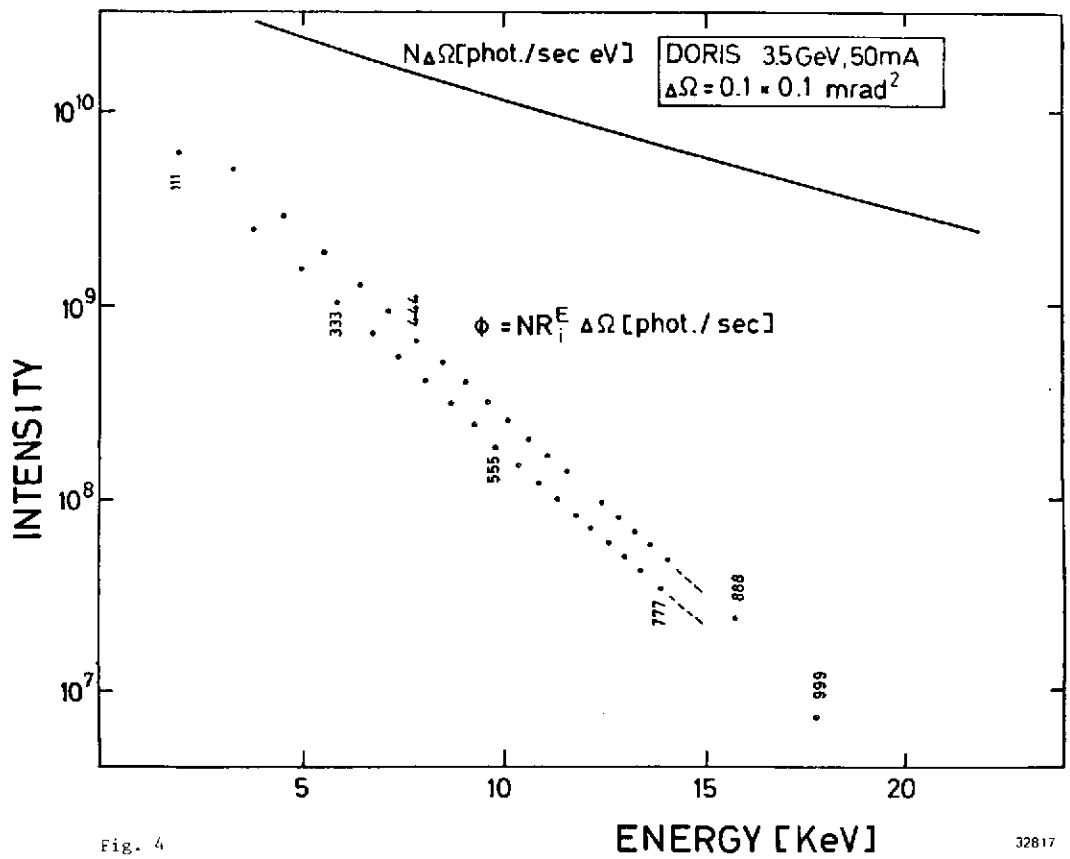
$N_{\Delta\Omega}$[phot./sec eV]
DORIS 3.5GeV,50mA
ΔΩ = 0.1 × 0.1 mrad²
$\Phi = NR_i^E\ \Delta\Omega$ [phot./sec]
INTENSITY
10^{10}
10^9
10^8
10^7
111
333
444
555
777
888
999
5
10
15
20
ENERGY [KeV]
32817

Fig. 4

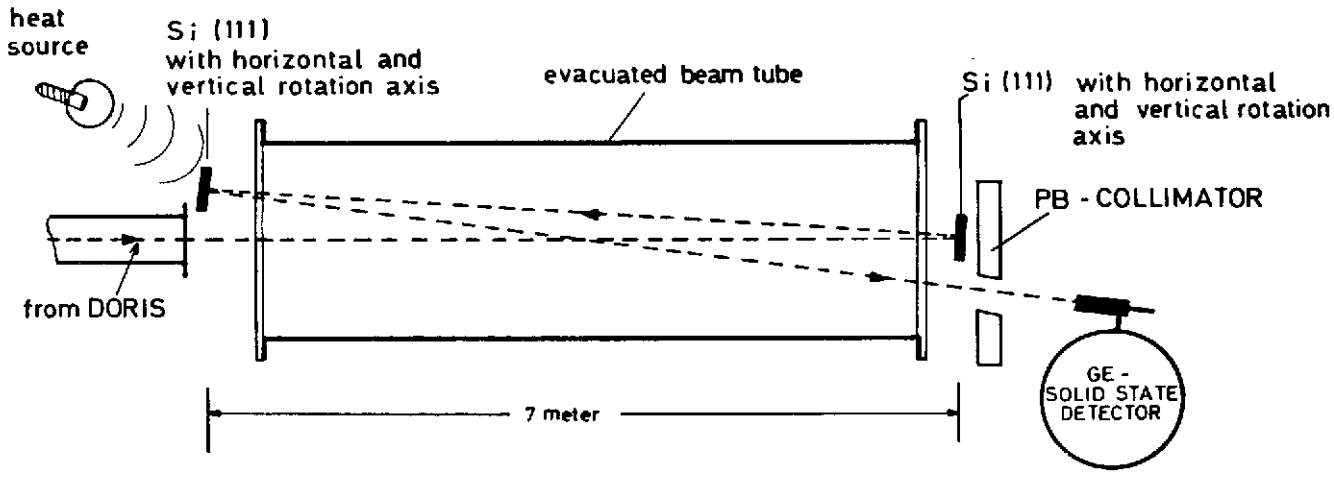

Fig. 5

32813

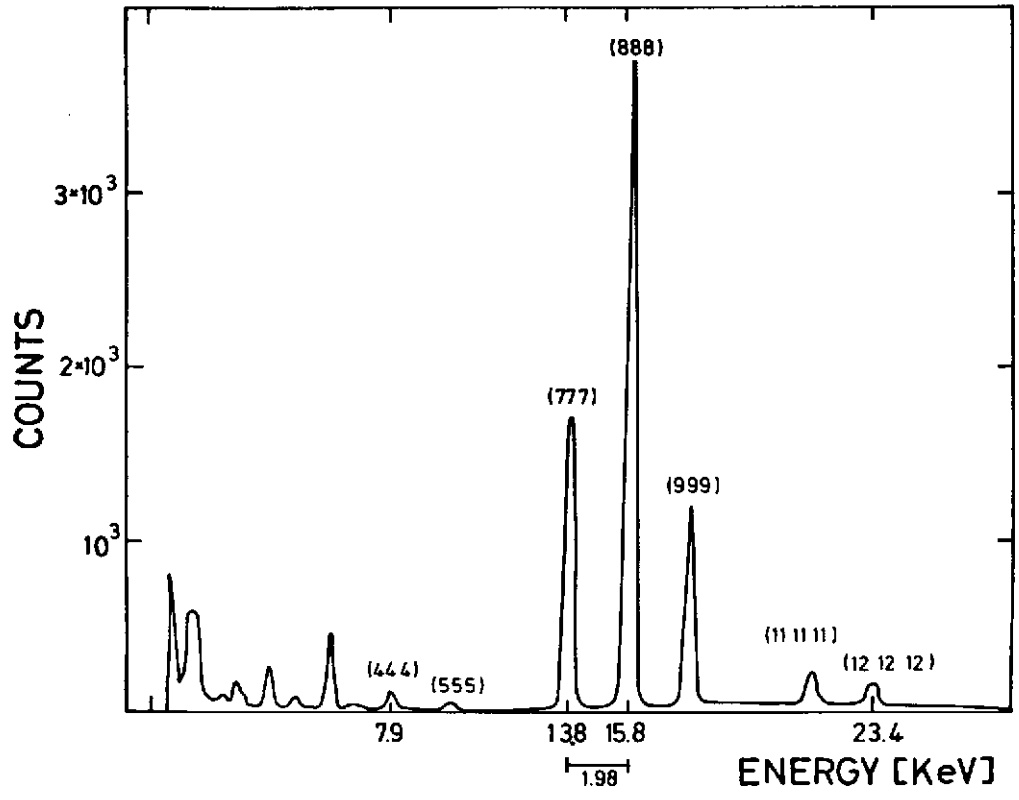

Fig. 6

32812

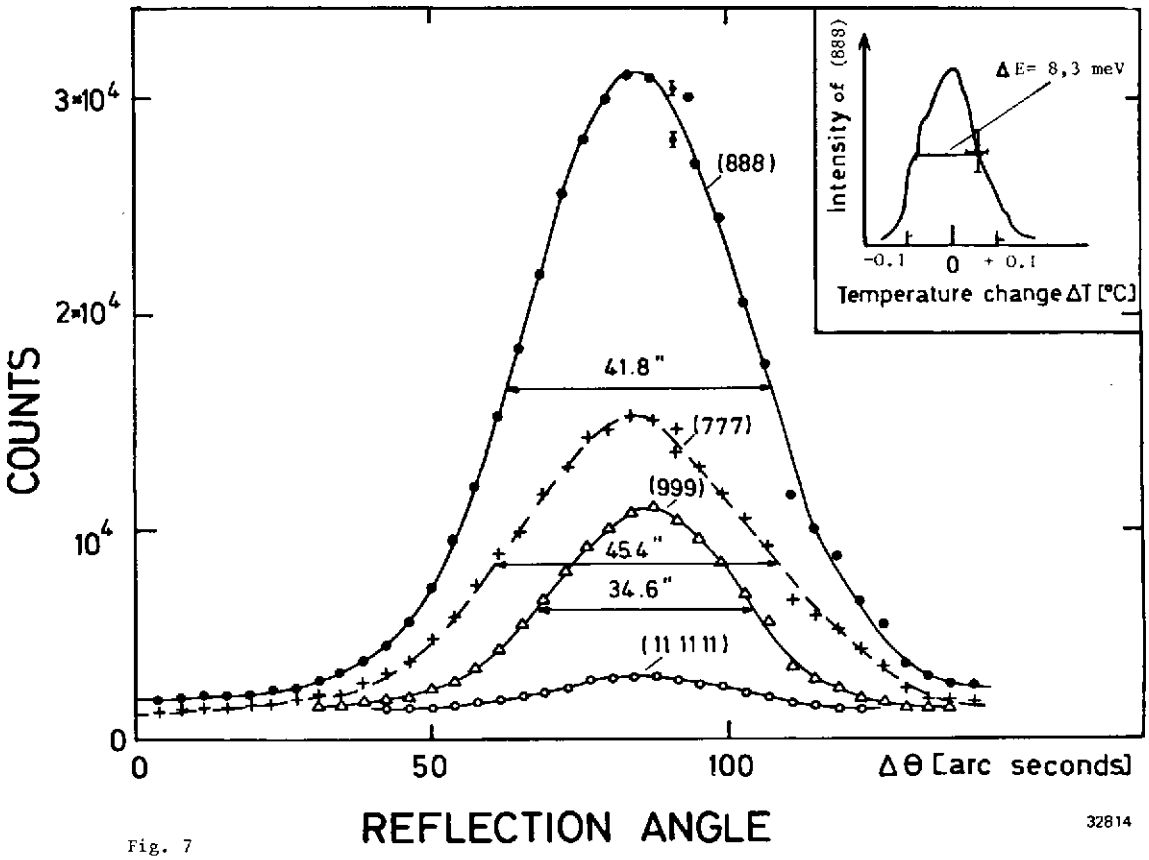
3×10^4
2×10^4
10^4
0
COUNTS
(888)
41.8"
(777)
(999)
45.4"
34.6"
(11 11 11)
0
50
100
Δ Θ [arc seconds]
REFLECTION ANGLE
Intensity of (888)
Δ E= 8,3 meV
-0.1
0
+ 0.1
Temperature change ΔT [°C]
32814

Fig. 7